Nano Research
2022, 15(8): 7559–7564

ISSN 1998-0124 CN 11-5974/O4
https://doi.org/10.1007/s12274-022-4383-6

Research Article

Utilization of cationic microporous metal-organic framework for efficient Xe/Kr separation

Lingshan Gong[1,§], Ying Liu[2,§], Junyu Ren[1], Abdullah M. Al-Enizi[3], Ayman Nafady[3], Yingxiang Ye[1] (✉), Zongbi Bao[2] (✉), and Shengqian Ma[1] (✉)

[1] *Department of Chemistry, University of North Texas, Denton, Texas 76201, USA*
[2] *Key Laboratory of Biomass Chemical Engineering of Ministry of Education, College of Chemical and Biological Engineering, Zhejiang University, Hangzhou 310027, China*
[3] *Department of Chemistry, College of Science, King Saud University, Riyadh 11451, Saudi Arabia*
[§] *Lingshan Gong and Ying Liu contributed equally to this work.*

Received: 20 January 2022 / **Revised:** 15 March 2022 / **Accepted:** 31 March 2022

ABSTRACT

The separation of xenon/krypton (Xe/Kr) mixtures plays a vital role in the industrial process of manufacturing high-purity xenon. Compared with energy-intensive cryogenic distillation, porous materials based on physical adsorption are very promising in the low-cost and energy-saving separation processes. Herein, we show that a cationic metal-organic framework (named as FJU-55) exhibits highly efficient Xe/Kr separation performance, which can be attributable to its uniform three-dimensional (3D) interconnection channels and the electro-positive features as the host framework. Moreover, FJU-55 demonstrates good Xe adsorption capacity of 1.41 mmol/g and excellent Xe/Kr selectivity of 10 (298 K and 100 kPa), together with a high Q_{st} value of 39.4 kJ/mol at low coverage area. The superior Xe/Kr separation performance of FJU-55 was further confirmed by the dynamic breakthrough experiments. Results obtained via molecular modeling studies have revealed that the suitable pore size and abundant accessible aromatic ligands in FJU-55 could offer strong multiple C–H···Xe interactions, which play a collaborative role in this challenging gas separation task.

KEYWORDS

gas separation, cationic metal-organic framework, microporous, xenon capture, krypton

Xenon (Xe) and krypton (Kr) are commercially valuable commodities, which are widely used in many fields such as commercial lighting, spacecraft propellants, medical imaging, and other basic researches [1–3]. Generally, xenon and krypton are present in extremely low concentrations in the atmosphere (Xe: 0.087 ppmv, Kr: 1.14 ppmv) [4]. Nowadays, commercial Xe and Kr were obtained as by-products from cryogenically distilled air, in which the gas mixture of 20/80 (v/v) Xe/Kr was found in the rare gas fractionation components [5]. Therefore, further distillation steps are required to manufacture high purity Xe or Kr by their difference in boiling point (Xe: −108.1 °C, Kr: −153.2 °C) [4]. It is well known that the cryogenic distillation is energy-intensive and thus accounts for a large part of the global energy consumption [6]. Recently, gas separation strategies based on porous solid adsorbents received enormous attention due to their low cost and energy-saving prospects [7, 8]. In this regard, traditional adsorbents like zeolites and activated carbon have been extensively investigated for Xe/Kr separation, however, the low adsorption capacity and/or poor selectivity have hindered their practical application [9, 10]. These limitations have prompted us to develop a new type of porous materials for effective Xe/Kr separation.

Recently, the emerging metal-organic frameworks (MOFs) have received widespread interest due to their large surface areas [11], well-defined pore features [12, 13], abundant structural tunability [14], and multifunctional potential applications (e.g., catalysis, proton conduction, sensing, and gas separation) [15–23]. It is known that noble gas shows similar single-atom spherical structure, low chemical reactivity, and weak polarizability (Xe: 40.44×10^{-25} cm^3; Kr: 24.84×10^{-25} cm^3) [5]. Besides, the subtle difference in kinetic diameters (Xe vs. Kr: 4.047 vs. 3.655 Å) makes the separation of Xe/Kr a great challenge [5, 24]. In 2011, based on high-throughput computational screening, Snurr and co-workers proposed that porous MOF has tubular channel with uniform small pore size (4–8 Å) and/or high concentration of polar groups decorated on the pore surface will promote Xe/Kr selectivity, thereby achieving efficient separation [25, 26]. Later, Thallapally et al. reported a Ca-based MOF (SBMOF-1) with the highest Xe adsorption capacity and remarkable Xe/Kr selectivity under the simulated nuclear fuel reprocessing conditions, which was ascribed to its suitable pore size and dense pore wall [27]. Moreover, recent studies have indicated that creating open metal sites or loading metal nanoparticles in porous MOF can polarize rare gas atoms, thereby increasing the adsorption capacity of Xe [28–34]. Therefore, by virtue of the concept of electric field across the pore space, we speculate that the charged host framework could enhance interactions between adsorbent and Xe molecule, consequently improving the adsorption capacity as well as the

Address correspondence to Yingxiang Ye, Yingxiang.Ye@unt.edu; Zongbi Bao, baozb@zju.edu.cn; Shengqian Ma, shengqian.ma@unt.edu

selectivity. Until now, the related research work based on this strategy has been sparse [35, 36], owing to the fact that the majority of the porous MOFs are electrically neutral framework.

In this work, we report a two-fold interpenetrated three-dimensional (3D) Cu-based MOF (named as FJU-55, $[Cu_6(\mu_3\text{-}OH)_2(CPT)_8]\cdot 2Br\cdot xG$, HCPT = 4-(4H-1,2,4-triazol-4-yl)benzoic acid; G = guest molecule) as a potential adsorbent for Xe/Kr separation. FJU-55 features 3D interconnected channels with uniform pore size as well as the electro-positive characteristic. As expected, FJU-55 exhibits a moderate Xe adsorption capacity (1.41 mmol/g) but high Xe/Kr selectivity (10) under ambient conditions. In addition, it gives high heat of adsorption (39.4 kJ/mol) at zero coverage. Furthermore, Grand Canonical Monte Carlo (GCMC) calculations reveal that suitable pore size and accessible aromatic ligands can facilitate strong multiple C–H···Xe interactions in the confined channels. Meanwhile, the superior Xe/Kr separation performance of FJU-55 was well supported in the dynamic breakthrough experiments. This work will suggest a new approach for the design and synthesis of porous MOFs in this burgeoning field of research.

The blue block-shaped crystals of FJU-55 (Fig. S1 in the Electronic Supplementary Material (ESM)) were prepared via solvothermal method, during which HCPT and $CuBr_2$ reacting in N,N-dimethylformamide (DMF)/MeOH/H_2O solvent mixture for 72 h at 85 °C. Single crystal X-ray diffraction reveals that FJU-55 crystallizes in monoclinic *P*2/*c* space group and forms a double interpenetrated 3D open framework. The asymmetric unit of FJU-55 contains six crystallographically independent Cu(II) ions, two μ_3-OH anions, eight CPT organic ligands, and two counter Br^- anions. As shown in Fig. 1(a), each Cu atom exhibits a five-coordinated mode with the square-pyramidal geometry. In this coordination environment, Cu1 is coordinated with three N atoms and two O atoms from four distinct organic ligands and one μ_3-OH group, with Cu2, Cu4, and Cu6 adopting the similar coordination mode as Cu1. Whereas Cu3 is bonded with two O and two N atoms from four individual CPT ligands, along with one O atom from the μ_3-OH group; Cu5 shows the same connection mode as Cu3. Three Cu atoms (Cu1, Cu2, and Cu3) around a μ_3-OH group are connected by four triazole and four carboxylic groups with bridging and single mode from eight independent CPT ligands to form an eight-connected trinuclear $[Cu_3(\mu_3\text{-}OH)(COO_2)_4(tz)_4]$ secondary building unit (SBU). Identically, Cu4, Cu5, and Cu6 also form the similar tri-nuclear Cu SBUs. Notably, these two tri-nuclear Cu SBUs are slightly different from each other in terms of the orientations of the carboxylic group coordinating with Cu2 and Cu4. The $[Cu_3(\mu_3\text{-}OH)]$ units are linked to six neighboring SBUs by CPT ligands, resulting in a triangle-tessellated two-dimensional (2D) layer structure along the *ab* plane, with a triangular window (Fig. 1(b)). After that, these layers are further connected by CPT ligands as pillars to form a two-fold interpenetrated three-dimensional open framework (Figs. 1(c)–1(e)). It is worth noting that the host framework of FJU-55 exhibits a 3D interconnected channel with uniform pore size (Fig. S2 in the ESM). If the $[Cu_3(\mu_3\text{-}OH)]$ SBUs were regard as 8-connected nodes, FJU-55 will form the hex network having a point symbol of $(3^6.4^{18}.5^3.6)$ [37]. After removal of the solvent molecules, the total accessible volume in FJU-55 is 31.3%, as calculated by PLATON software [38].

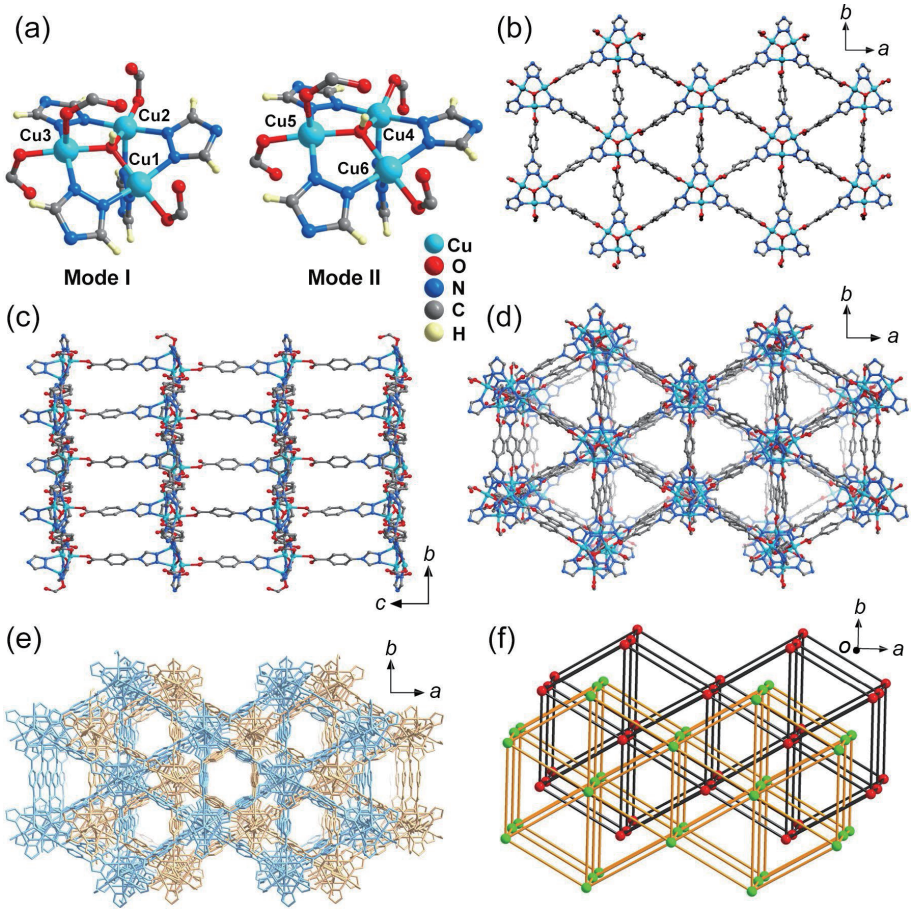

Figure 1 Structure of FJU-55 showing (a) the two types of trinuclear Cu(II) SBUs. (b) The construction of 2D layer structure of $Cu_3(\mu_3\text{-}OH)(CPT)_3$ in FJU-55. (c) and (d) The pillar CPT ligands connect the 2D layer to form 3D open framework along the *a* and *c* axis, respectively. (e) The two-fold interpenetrated 3D open framework with one-dimensional (1D) channel viewed along the *c*-axis direction. (f) The host framework simplified to 2-fold interpenetrated hex network. Hydrogen atoms and counter anions have been omitted for clarity.

Powder X-ray diffraction (PXRD) measurement confirmed the purity of the as-synthesized MOF, showing a good match between the calculated and experimental patterns (Fig. S5 in the ESM). From the thermo gravimetric analysis (TGA) curve, the as-synthesized sample exhibits a continuous weight loss from room temperature to 250 °C, after which the host framework begins to decompose (Fig. S7 in the ESM). Meanwhile, the *in-suit* variable-temperature PXRD patterns further demonstrated that the host framework remains intact until 250 °C (Fig. S6 in the ESM).

To examine the permanent porosity features of FJU-55, the fresh prepared sample was exchanged with anhydrous methanol and degassed overnight at 60 °C under high vacuum. As shown in Fig. 2(a), the N_2 sorption isotherms at 77 K of FJU-55 displayed a fully reversible type-I behavior with the saturated uptake value of 121 cm^3/g. The corresponding pore volume was calculated to be 0.19 cm^3/g. The Brunauer–Emmett–Teller (BET) and Langmuir surface areas were found to be 377 and 498 m^2/g, respectively, based on the N_2 adsorption isotherms. In addition, FJU-55 shows a narrow pore size distribution (PSD) with the centered at 5.6 and 8.6 Å, respectively, by employing the no-local density functional theory (NLDFT) model [39], which is close to the pore aperture size determined by the crystal structure (Fig. S2 in the ESM).

The establishment of permanent porous structure and suitable pore aperture sizes of FJU-55 prompted us to further investigate its Xe/Kr separation performance in detail. Single-component isotherms of Xe and Kr were performed on Micromeritics ASAP 2460 adsorption instrument. As show in Fig. 2(b), the uptake capacities of xenon and krypton are 1.41 mmol/g (1.96 mmol/g) and 0.62 mmol/g (0.94 mmol/g) at 298 K (273 K) and 100 kPa, respectively. At ambient conditions, the Xe uptake value in FJU-55 is lower than those MOFs with larger surface areas and high-density open metal sites (e.g., 3.4 mmol/g for HKUST-1, 5.0 mmol/g for Cu-ATC, and 4.2 mmol/g for Ni-MOF-74) [28, 34, 40], and comparable with some benchmark materials, such as CROFOUR-1-Ni (1.77 mmol/g) [41], $Co_3(C_4O_4)_2(OH)_2$ (1.35 mmol/g) [42], and SBMOF-1 (1.38 mmol/g) [27], and even higher than those of $Sr_4(TCPE)_2$ (1.1 mmol/g) [43] and FMOFCu (0.46 mmol/g) [44]. Notably, the adsorption isotherm of Xe rapidly increases when compared with Kr in the low-pressure region, which suggests that FJU-55 is a promising candidate for Xe/Kr separation.

To compare the binding affinities of Xe and Kr in FJU-55, the isosteric heat of adsorption (Q_{st}) was determined by using the well-defined Virial method based on their corresponding 273 and 298 K adsorption isotherms. The zero coverage Q_{st} was found to be of 39.4 and 14.4 kJ/mol for Xe and Kr, respectively, which indicates stronger interactions between host framework and guest Xe atoms. The Q_{st} value of Xe in FJU-55 is only slightly lower than the benchmark material $Co_3(C_4O_4)_2(OH)_2$ (43.6 kJ/mol) [42], and surpasses a majority of top performing porous materials, including CROFOUR-1-Ni (37.4 kJ/mol) [41], MOF-Cu-H (33.4 kJ/mol) [45], and SBMOF-2 (26.4 kJ/mol) [46]. More importantly, the difference of adsorption enthalpies (ΔQ_{st}) between Xe and Kr in FJU-55 is up to 25 kJ/mol, defined as $\Delta Q_{st} = Q_{st}$ (Xe) − Q_{st} (Kr), which is among the highest level and higher than the majority of the reported porous materials (Fig. 2(c) and Table S2 in the ESM) [31, 42, 45, 47–54].

It has further prompted us to investigate the Xe/Kr separation selectivity by considering their remarkably different interactions with host framework. The ideal adsorbed solution theory (IAST) [55] was employed to calculate the adsorption selectivity of Xe/Kr (20/80) mixture at 273 and 298 K under different pressures. In Fig. 2(d), it shows that the Xe/Kr selectivity ranges from 16 to 10 at 298 K under pressure from 0 to 100 kPa. Although the Xe/Kr selectivity of FJU-55 is lower than some benchmark materials [41, 42, 56, 57], it still higher than MOF-801 (8.3) [52], HKUST-1 (6.5) [2], NKMOF-1-Ni (5.2) [58], and NU-403 (2.8) [59] (Fig. 2(e)). Similarly, at 273 K, the Xe/Kr selectivity range is also found from 50 to 16, which is also high compared with most benchmark materials. These results endue that the FJU-55 unfolds Xe/Kr separation proficiency.

To further evaluate the separation ability of FJU-55 toward

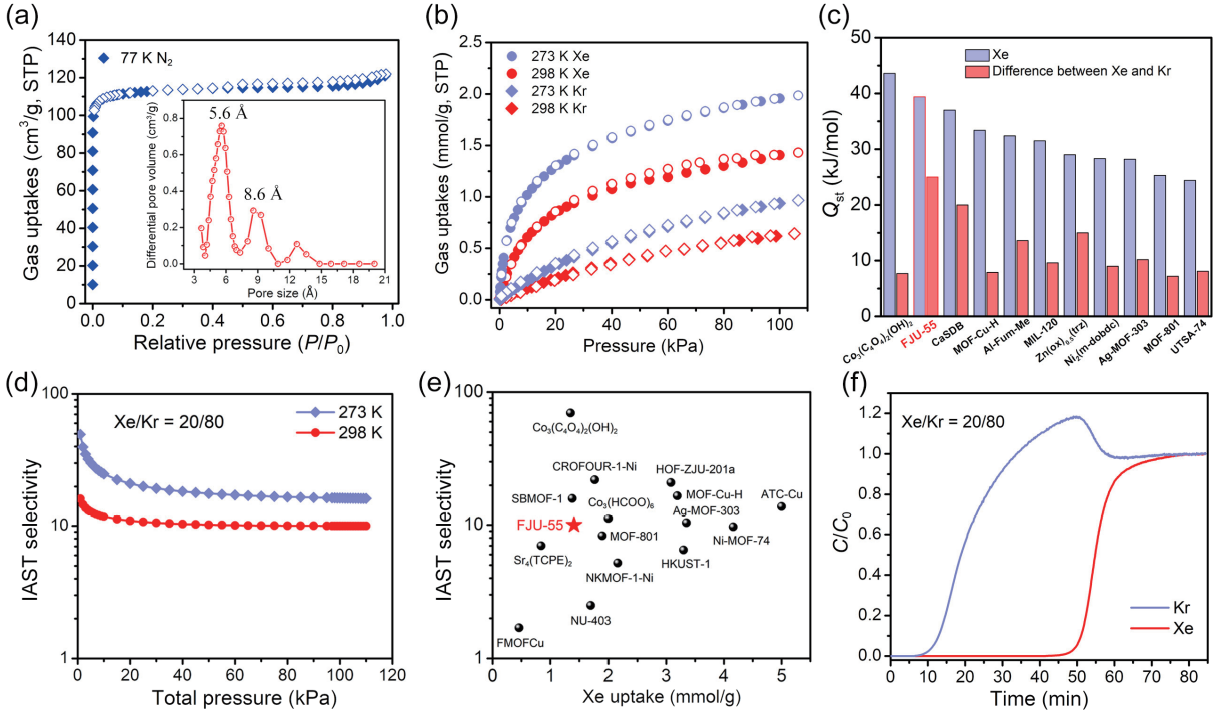

Figure 2 (a) Nitrogen adsorption isotherms of FJU-55 at 77 K. Inset: the corresponding PSD. (b) Xenon and krypton adsorption isotherms of FJU-55 at 273 and 298 K, respectively. (c) Comparison of the Q_{st} of FJU-55 with some representative porous materials. (d) The IAST adsorption selectivity of FJU-55 for Xe/Kr (20/80) at 273 and 298 K, respectively. (e) Comparison of Xenon uptake and IAST selectivity for Xe/Kr (20/80, v/v) among the reported porous materials under ambient condition. (f) Dynamic breakthrough curves of FJU-55 for Xe/Kr (20/80) gas mixture under 298 K and 1 bar.

Xe/Kr mixtures in real applications, we performed a laboratory-scale dynamic column breakthrough experiment. In doing so, the gas mixtures of Xe/Kr (20/80, v/v) were flowed at a 1.6 mL/min over a packed column under ambient conditions. As depicted in Fig. 2(f), the gas mixtures passing through the packed column can be effectively separated, as the signal of Kr was quickly detected (~ 7 min), while the gas of Xe was not found until 42 min, indicating the ultra-long retention time of FJU-55 (~ 35 min). According to the breakthrough curve, the dynamic Xe capture capacities (q_{Xe}) and separation factors ($\alpha_{Xe/Kr}$) were calculated to be of 1.3 mol/kg and 5.6, respectively. Moreover, the productivity of high-purity Kr (> 99.9%) of FJU-55 can reach up to 2.2 mol/kg under a given cycle, which is comparable with SMOF-PFSIX-1 (1.7 mol/kg) [36] and even higher than that of $Co_3(C_4O_4)_2(OH)_2$ (0.35 mol/kg) [42] under the similar conditions. To further investigate the recyclability of MOF for Xe/Kr separation, we carried out three cycles of mixed gas dynamic breakthrough experiments. The results show that FJU-55 maintained the same breakthrough time and dynamic capture amount of Xe as the initial one (Figs. S16 and S17 in the ESM). Moreover, FJU-55 still retains its intact structure after dynamic breakthrough experiments, as confirmed by the PXRD patterns (Fig. S18 in the ESM).

To gain insight into the adsorption and separation mechanism of xenon and krypton in FJU-55, GCMC simulations were performed to calculate the density distribution, binding site, and energy of these gases in FJU-55 at the molecular level (details were showed in the ESM). As illustrated in Fig. S19 in the ESM, xenon and krypton were adsorbed in the similar positions, while the density of Xe is obviously higher than the corresponding Kr. This result is consistent with the adsorption isotherms in which the absorption capacity of Xe is higher than that of Kr. After that, the GCMC simulations were also used to investigate the host–guest interactions between Xe or Kr and the host framework of FJU-55. According to the calculation results, it was found that the Xe atom was located in the midpoint of the channel along the *b*-axis (Fig. 3(a)). In contrast, the binding site of Kr is slightly off from the center of the channel while closer to one of the host frameworks (Fig. 3(b)). Both of them interact with the channel wall formed by the aromatic rings mainly through the van der Waals interactions. The binding energy of Xe was found to be 7.1 kcal/mol, which is higher than the corresponding value of Kr (5.2 kcal/mol). This finding clearly established that the interaction between Xe and the host framework is stronger than that of Kr, owing to the fact that Xe has a larger atomic radius and stronger polarizability. Moreover, this result is in a good agreement with the low coverage isosteric heat of adsorption. Ultimately, the difference in the interaction behavior between the gas molecule and the host framework is likely to be the key factor in achieving outstanding Xe/Kr separation performance.

In conclusion, a double interpenetrated cationic MOF with uniform 3D interconnecting channels, which is formed by trinuclear Cu nodes and CPT ligands, exhibits excellent separation performances towards Xe/Kr mixtures and even surpass some benchmark porous materials. Moreover, the Xe/Kr separation performances of FJU-55 were further supported by modeling studies and dynamic breakthrough experiments. In future work, we will focus on systematically evaluating the effect of pore size and the host frameworks' charge features on the Xe/Kr separation performance of porous MOFs.

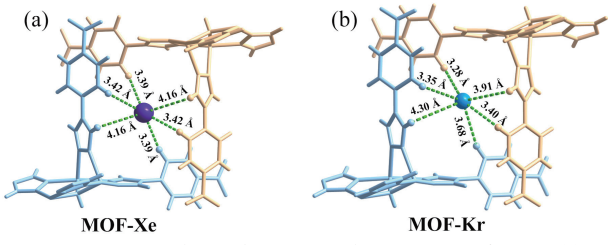

Figure 3 GCMC simulation the primary absorption site of xenon (a) and krypton (b) in FJU-55.

Acknowledgements

The authors acknowledge the Robert A. Welch Foundation (No. B-0027) for financial support of this work. We would also like to acknowledge the partial support from the National Natural Science Foundation of China (No. 21978254) and Researchers Supporting Program (No. RSP-2022/55) at King Saud University, Riyadh, Saudi Arabia.

Electronic Supplementary Material: Supplementary material (attached with all the supporting figures mentioned in this work) is available in the online version of this article at https://doi.org/10.1007/s12274-022-4383-6.

References

[1] Lane, G. A.; Nahrwold, M. L.; Tait, A. R.; Taylor-Busch, M.; Cohen, P. J.; Beaudoin, A. R. Anesthetics as teratogens: Nitrous oxide is fetotoxic, xenon is not. *Science* **1980**, *210*, 899–901.

[2] Banerjee, D.; Cairns, A. J.; Liu, J.; Motkuri, R. K.; Nune, S. K.; Fernandez, C. A.; Krishna, R.; Strachan, D. M.; Thallapally, P. K. Potential of metal-organic frameworks for separation of xenon and krypton. *Acc. Chem. Res.* **2015**, *48*, 211–219.

[3] Banerjee, D.; Simon, C. M.; Elsaidi, S. K.; Haranczyk, M.; Thallapally, P. K. Xenon gas separation and storage using metal-organic frameworks. *Chem* **2018**, *4*, 466–494.

[4] Kerry, F. G. *Industrial Gas Handbook*: *Gas Separation and Purification*; CRC Press: Boca Raton, 2007.

[5] Li, J. R.; Kuppler, R. J.; Zhou, H. C. Selective gas adsorption and separation in metal-organic frameworks. *Chem. Soc. Rev.* **2009**, *38*, 1477–1504.

[6] Sholl, D. S.; Lively, R. P. Seven chemical separations to change the world. *Nature* **2016**, *532*, 435–437.

[7] Chu, S.; Cui, Y.; Liu, N. The path towards sustainable energy. *Nat. Mater.* **2017**, *16*, 16–22.

[8] Ye, Y. X.; Xian, S. K.; Cui, H.; Tan, K.; Gong, L. S.; Liang, B.; Pham, T.; Pandey, H.; Krishna, R.; Lan, P. C. et al. Metal-organic framework based hydrogen-bonding nanotrap for efficient acetylene storage and separation. *J. Am. Chem. Soc.* **2022**, *144*, 1681–1689.

[9] Bazan, R. E.; Bastos-Neto, M.; Moeller, A.; Dreisbach, F.; Staudt, R. Adsorption equilibria of O_2, Ar, Kr and Xe on activated carbon and zeolites: Single component and mixture data. *Adsorption* **2011**, *17*, 371–383.

[10] Munakata, K.; Fukumatsu, T.; Yamatsuki, S.; Tanaka, K.; Nishikawa, M. Adsorption equilibria of krypton, xenon, nitrogen and their mixtures on molecular sieve 5A and activated charcoal. *J. Nucl. Sci. Technol.* **1999**, *36*, 818–829.

[11] Chen, Z. J.; Li, P. H.; Anderson, R.; Wang, X. J.; Zhang, X.; Robison, L.; Redfern, L. R.; Moribe, S.; Islamoglu, T.; Gómez-Gualdrón, D. A. et al. Balancing volumetric and gravimetric uptake in highly porous materials for clean energy. *Science* **2020**, *368*, 297–303.

[12] Lin, R. B.; Zhang, Z. J.; Chen, B. L. Achieving high performance metal-organic framework materials through pore engineering. *Acc. Chem. Res.* **2021**, *54*, 3362–3376.

[13] Cui, H.; Ye, Y. X.; Liu, T.; Alothman, Z. A.; Alduhaish, O.; Lin, R. B.; Chen, B. L. Isoreticular microporous metal-organic frameworks for carbon dioxide capture. *Inorg. Chem.* **2020**, *59*, 17143–17148.

[14] Furukawa, H.; Cordova, K. E.; O'Keeffe, M.; Yaghi, O. M. The chemistry and applications of metal-organic frameworks. *Science* **2013**, *341*, 1230444.

[15] Jiao, L.; Wang, J. X.; Jiang, H. L. Microenvironment modulation in metal-organic framework-based catalysis. *Acc. Mater. Res.* **2021**, *2*, 327–339.
[16] Ye, Y. X.; Gong, L. S.; Xiang, S. C.; Zhang, Z. J.; Chen, B. L. Metal-organic frameworks as a versatile platform for proton conductors. *Adv. Mater.* **2020**, *32*, 1907090.
[17] Li, H. Y.; Zhao, S. N.; Zang, S. Q.; Li, J. Functional metal-organic frameworks as effective sensors of gases and volatile compounds. *Chem. Soc. Rev.* **2020**, *49*, 6364–6401.
[18] Lin, R. B.; Xiang, S. C.; Zhou, W.; Chen, B. L. Microporous metal-organic framework materials for gas separation. *Chem* **2020**, *6*, 337–363.
[19] Ye, Y. X.; Ma, Z. L.; Chen, L. J.; Lin, H. Z.; Lin, Q. J.; Liu, L. Z.; Li, Z. Y.; Chen, S. M.; Zhang, Z. J.; Xiang, S. C. Microporous metal-organic frameworks with open metal sites and π-Lewis acidic pore surfaces for recovering ethylene from polyethylene off-gas. *J. Mater. Chem. A* **2018**, *6*, 20822–20828.
[20] Ye, Y. X.; Ma, Z. L.; Lin, R. B.; Krishna, R.; Zhou, W.; Lin, Q. J.; Zhang, Z. J.; Xiang, S. C.; Chen, B. L. Pore space partition within a metal-organic framework for highly efficient C_2H_2/CO_2 separation. *J. Am. Chem. Soc.* **2019**, *141*, 4130–4136.
[21] Ye, Y. X.; Guo, W. G.; Wang, L. H.; Li, Z. Y.; Song, Z. J.; Chen, J.; Zhang, Z. J.; Xiang, S. C.; Chen, B. L. Straightforward loading of imidazole molecules into metal-organic framework for high proton conduction. *J. Am. Chem. Soc.* **2017**, *139*, 15604–15607.
[22] Wang, Q. J.; Ke, T.; Yang, L. F.; Zhang, Z. Q.; Cui, X. L.; Bao, Z. B.; Ren, Q. L.; Yang, Q. W.; Xing, H. B. Separation of Xe from Kr with record selectivity and productivity in anion-pillared ultramicroporous materials by inverse size-sieving. *Angew. Chem., Int. Ed.* **2020**, *59*, 3423–3428.
[23] Zheng, F.; Guo, L. D.; Chen, R. D.; Chen, L. H.; Zhang, Z. G.; Yang, Q. W.; Yang, Y. W.; Su, B. G.; Ren, Q. L.; Bao, Z. B. Shell-like xenon nano-traps within angular anion-pillared layered porous materials for boosting Xe/Kr separation. *Angew. Chem., Int. Ed.* **2022**, *61*, e202116686.
[24] Chen, L. J.; Reiss, P. S.; Chong, S. Y.; Holden, D.; Jelfs, K. E.; Hasell, T.; Little, M. A.; Kewley, A.; Briggs, M. E.; Stephenson, A. et al. Separation of rare gases and chiral molecules by selective binding in porous organic cages. *Nat. Mater.* **2014**, *13*, 954–960.
[25] Ryan, P.; Farha, O. K.; Broadbelt, L. J.; Snurr, R. Q. Computational screening of metal-organic frameworks for xenon/krypton separation. *AIChE J.* **2011**, *57*, 1759–1766.
[26] Sikora, B. J.; Wilmer, C. E.; Greenfield, M. L.; Snurr, R. Q. Thermodynamic analysis of Xe/Kr selectivity in over 137,000 hypothetical metal-organic frameworks. *Chem. Sci.* **2012**, *3*, 2217–2223.
[27] Banerjee, D.; Simon, C. M.; Plonka, A. M.; Motkuri, R. K.; Liu, J.; Chen, X. Y.; Smit, B.; Parise, J. B.; Haranczyk, M.; Thallapally, P. K. Metal-organic framework with optimally selective xenon adsorption and separation. *Nat. Commun.* **2016**, *7*, 11831.
[28] Thallapally, P. K.; Grate, J. W.; Motkuri, R. K. Facile xenon capture and release at room temperature using a metal-organic framework: A comparison with activated charcoal. *Chem. Commun.* **2012**, *48*, 347–349.
[29] Liu, J.; Strachan, D. M.; Thallapally, P. K. Enhanced noble gas adsorption in Ag@MOF-74Ni. *Chem. Commun.* **2014**, *50*, 466–468.
[30] Perry, J. J.; Teich-McGoldrick, S. L.; Meek, S. T.; Greathouse, J. A.; Haranczyk, M.; Allendorf, M. D. Noble gas adsorption in metal-organic frameworks containing open metal sites. *J. Phys. Chem. C* **2014**, *118*, 11685–11698.
[31] Wang, H. Z.; Shi, Z. L.; Yang, J. J.; Sun, T.; Rungtaweevoranit, B.; Lyu, H.; Zhang, Y. B.; Yaghi, O. M. Docking of Cu^{I} and Ag^{I} in metal-organic frameworks for adsorption and separation of xenon. *Angew. Chem., Int. Ed.* **2021**, *60*, 3417–3421.
[32] Wang, Y. L.; Liu, W.; Bai, Z. L.; Zheng, T.; Silver, M. A.; Li, Y. X.; Wang, Y. X.; Wang, X.; Diwu, J.; Chai, Z. F. et al. Employing an unsaturated Th^{4+} site in a porous thorium-organic framework for Kr/Xe uptake and separation. *Angew. Chem., Int. Ed.* **2018**, *57*, 5783–5787.
[33] Pei, J. Y.; Gu, X. W.; Liang, C. C.; Chen, B. L.; Li, B.; Qian, G. D. Robust and radiation-resistant hofmann-type metal-organic frameworks for record xenon/krypton separation. *J. Am. Chem. Soc.* **2022**, *144*, 3200–3209.
[34] Niu, Z.; Fan, Z. W.; Pham, T.; Verma, G.; Forrest, K. A.; Space, B.; Thallapally, P. K.; Al-Enizi, A. M.; Ma, S. Q. Self-adjusting metal-organic framework for efficient capture of trace xenon and krypton. *Angew. Chem., Int. Ed.* **2022**, *61*, e202117807.
[35] Liu, B. Y.; Gong, Y. J.; Wu, X. N.; Liu, Q.; Li, W.; Xiong, S. S.; Hu, S.; Wang, X. L. Enhanced xenon adsorption and separation with an anionic indium-organic framework by ion exchange with Co^{2+}. *RSC Adv.* **2017**, *7*, 55012–55019.
[36] Liu, Y.; Dai, J. J.; Guo, L. D.; Zhang, Z. G.; Yang, Y. W.; Yang, Q. W.; Ren, Q. L.; Bao, Z. B. Porous hydrogen-bonded frameworks assembled from metal-nucleobase entities for Xe/Kr separation. *CCS Chem.* **2022**, *4*, 381–388.
[37] Blatov, V. A.; Shevchenko, A. P.; Proserpio, D. M. Applied topological analysis of crystal structures with the program package ToposPro. *Cryst. Growth Des.* **2014**, *14*, 3576–3586.
[38] Spek, A. L. Single-crystal structure validation with the program *PLATON*. *J. Appl. Cryst.* **2003**, *36*, 7–13.
[39] Ravikovitch, P. I.; Vishnyakov, A.; Russo, R.; Neimark, A. V. Unified approach to pore size characterization of microporous carbonaceous materials from N_2, Ar, and CO_2 adsorption isotherms. *Langmuir* **2000**, *16*, 2311–2320.
[40] Soleimani Dorcheh, A.; Denysenko, D.; Volkmer, D.; Donner, W.; Hirscher, M. Noble gases and microporous frameworks; from interaction to application. *Microporous Mesoporous Mater.* **2012**, *162*, 64–68.
[41] Mohamed, M. H.; Elsaidi, S. K.; Pham, T.; Forrest, K. A.; Schaef, H. T.; Hogan, A.; Wojtas, L.; Xu, W. Q.; Space, B.; Zaworotko, M. J. et al. Hybrid ultra-microporous materials for selective xenon adsorption and separation. *Angew. Chem., Int. Ed.* **2016**, *55*, 8285–8289.
[42] Li, L. Y.; Guo, L. D.; Zhang, Z. G.; Yang, Q. W.; Yang, Y. W.; Bao, Z. B.; Ren, Q. L.; Li, J. A robust squarate-based metal-organic framework demonstrates record-high affinity and selectivity for xenon over krypton. *J. Am. Chem. Soc.* **2019**, *141*, 9358–9364.
[43] Xiong, J. B.; Li, A. L.; Fan, Y. L.; Xu, Z. Z.; Feng, H.; Gao, Q.; Fan, Q. W.; He, Y.; Gao, Z.; Luo, F. Creating uniform pores for xenon/krypton and acetylene/ethylene separation on a strontium-based metal-organic framework. *J. Solid State Chem.* **2020**, *288*, 121337.
[44] Fernandez, C. A.; Liu, J.; Thallapally, P. K.; Strachan, D. M. Switching Kr/Xe selectivity with temperature in a metal-organic framework. *J. Am. Chem. Soc.* **2012**, *134*, 9046–9049.
[45] Xiong, S. S.; Gong, Y. J.; Hu, S. L.; Wu, X. N.; Li, W.; He, Y. B.; Chen, B. L.; Wang, X. L. A microporous metal-organic framework with commensurate adsorption and highly selective separation of xenon. *J. Mater. Chem. A* **2018**, *6*, 4752–4758.
[46] Chen, X. Y.; Plonka, A. M.; Banerjee, D.; Krishna, R.; Schaef, H. T.; Ghose, S.; Thallapally, P. K.; Parise, J. B. Direct observation of Xe and Kr adsorption in a Xe-selective microporous metal-organic framework. *J. Am. Chem. Soc.* **2015**, *137*, 7007–7010.
[47] Yu, G. L.; Liu, Y. Q.; Zou, X. Q.; Zhao, N.; Rong, H. Z.; Zhu, G. S. A nanosized metal-organic framework with small pores for kinetic xenon separation. *J. Mater. Chem. A* **2018**, *6*, 11797–11803.
[48] Yan, Z. T.; Gong, Y. J.; Yang, C. T.; Wu, X. N.; Liu, B. Y.; Liu, Q.; Xiong, S. S.; Peng, S. M. Pore size reduction by methyl function in aluminum-based metal-organic frameworks for xenon/krypton separation. *Cryst. Growth Des.* **2020**, *20*, 8039–8046.
[49] Zhang, P. X.; Zhong, Y.; Yao, Q.; Liu, X.; Zhang, Y.; Wang, J.; Deng, Q.; Zeng, Z. L.; Deng, S. G. Robust ultramicroporous metal-organic framework with rich hydroxyl-decorated channel walls for highly selective noble gas separation. *J. Chem. Eng. Data* **2020**, *65*, 4018–4023.
[50] Yu, L.; Xiong, S. S.; Lin, Y. H.; Li, L. Y.; Peng, J. J.; Liu, W.; Huang, X. X.; Wang, H.; Li, J. Tuning the channel size and structure flexibility of metal-organic frameworks for the selective adsorption of noble gases. *Inorg. Chem.* **2019**, *58*, 15025–15028.
[51] Kapelewski, M. T.; Oktawiec, J.; Runčevski, T.; Gonzalez, M. I.; Long, J. R. Separation of xenon and krypton in the metal-organic

frameworks M_2(m-dobdc) (M = Co, Ni). *Isr. J. Chem.* **2018**, *58*, 1138–1143.

[52] Yan, Z. T.; Gong, Y. J.; Chen, B. H.; Wu, X. N.; Liu, Q.; Cui, L. L.; Xiong, S. S.; Peng, S. M. Methyl functionalized Zr-Fum MOF with enhanced xenon adsorption and separation. *Sep. Purif. Technol.* **2020**, *239*, 116514.

[53] Tao, Y.; Fan, Y. L.; Xu, Z. Z.; Feng, X. F.; Krishna, R.; Luo, F. Boosting selective adsorption of Xe over Kr by double-accessible open-metal site in metal-organic framework: Experimental and theoretical research. *Inorg. Chem.* **2020**, *59*, 11793–11800.

[54] Luo, S. H.; Ma, F. Y.; Wang, X.; Yuan, M. J.; Chen, L. H.; Qiu, S. K.; Tang, Q.; Wang, S. Uptake and separation of Xe and Kr by a zeolitic imidazolate framework with a desirable pore window. *J. Radioanal. Nucl. Chem.* **2020**, *324*, 1275–1281.

[55] Myers, A. L.; Prausnitz, J. M. Thermodynamics of mixed-gas adsorption. *AIChE J.* **1965**, *11*, 121–127.

[56] Wang, H.; Yao, K. X.; Zhang, Z. J.; Jagiello, J.; Gong, Q. H.; Han, Y.; Li, J. The first example of commensurate adsorption of atomic gas in a MOF and effective separation of xenon from other noble gases. *Chem. Sci.* **2014**, *5*, 620–624.

[57] Liu, Y.; Wu, H.; Guo, L. D.; Zhou, W.; Zhang, Z. G.; Yang, Q. W.; Yang, Y. W.; Ren, Q. L.; Bao, Z. B. Hydrogen-bonded metal-nucleobase frameworks for efficient separation of xenon and krypton. *Angew. Chem., Int. Ed.* **2022**, *61*, e202117609.

[58] Wang, T.; Peng, Y. L.; Lin, E.; Niu, Z.; Li, P. F.; Ma, S. Q.; Zhao, P.; Chen, Y.; Cheng, P.; Zhang, Z. J. Robust bimetallic ultramicroporous metal-organic framework for separation and purification of noble gases. *Inorg. Chem.* **2020**, *59*, 4868–4873.

[59] Idrees, K. B.; Chen, Z. J.; Zhang, X.; Mian, M. R.; Drout, R. J.; Islamoglu, T.; Farha, O. K. Tailoring pore aperture and structural defects in zirconium-based metal-organic frameworks for krypton/xenon separation. *Chem. Mater.* **2020**, *32*, 3776–3782.